Drag-induced radiative energy loss from semihard heavy quarks

Raktim Abir and Abhijit Majumder
Department of Physics and Astronomy, Wayne State University, 666 W. Hancock Street, Detroit, Michigan 48201, USA
(Received 9 September 2015; revised manuscript received 24 July 2016; published 7 November 2016)

The case of gluon bremsstrahlung off a heavy quark in extended nuclear matter is revisited within the higher twist formalism. In particular, the in-medium modification of "semihard" heavy quarks is studied, where the momentum of the heavy quark is larger but comparable to the mass of the heavy quark ($p \gtrsim M$). In contrast to all prior calculations, where the gluon emission spectrum is entirely controlled by the transverse momentum diffusion parameter ($\hat{q}$), both for light and heavy quarks, in this work, we demonstrate that the gluon emission spectrum for a heavy quark (unlike that for light flavors) is also sensitive to $\hat{e}$, which so far has been used to quantify the amount of *light-cone* drag experienced by a parton. This mass dependent effect, due to the *non-light-like* momentum of a semihard heavy quark, leads to an additional energy loss term for heavy quarks, while resulting in a negligible modification of light flavor (and high energy heavy flavor) energy loss. This result can be used to estimate the value of this subleading nonperturbative jet transport parameter ($\hat{e}$) from heavy flavor suppression in ultrarelativistic heavy-ion collisions.

DOI: 10.1103/PhysRevC.94.054902

I. INTRODUCTION

The unprecedented center-of-mass energies available at the Large Hadron Collider have opened new windows for the exploration of extreme nuclear matter through high energy jets [1–6]. While a large portion of the available data on leading (and next-to-leading) particle suppression in the light flavor sector has been theoretically described using factorized pQCD based calculations of jet modification [7,8], heavy quarks have remained somewhat of a challenge [9]. This is especially true in the semihard sector, where the momentum of the heavy quark is larger but comparable to its mass $p \gtrsim m_Q$. We distinguish this region from that of slow heavy quarks, where $p \lesssim m_Q$, which appear to be thermalized with the bulk medium, and fast heavy quarks, with $p \gg m_Q$ which engender energy loss and suppression similar to light quarks.

The so called "heavy-quark puzzle" had already begun to manifest itself in measurements of the suppression of high transverse momentum (high-p_T) nonphotonic electrons at the Relativistic Heavy-Ion Collider (RHIC). Measurements by both the STAR [10] and PHENIX [11] detectors showed a slightly higher suppression than expected, based on a calculation that included both drag and radiative loss [8,12,13]. This trend has continued at the Large Hadron Collider (LHC) where the ALICE experiment has measured D and B meson suppression separately, and finds a larger than expected suppression in the semihard regime of heavy-quark momentum (we note that the case is not very clear for B-meson suppression which has so far only been presented as p_T integrated points) [14,15].

A considerable amount of theoretical work, within pQCD based formalisms (which we limit ourselves to), has been devoted to understand this larger than expected suppression of single electrons or heavy mesons arising from the fragmentation of a heavy quark [9,16]. However, most of these may be understood as falling in two categories: Calculations that have extended the base formalism of radiated energy loss for light flavors to include mass dependent terms, as well as a drag term to include the prominent role played by drag in heavy flavor energy loss [8,17–21]. Calculations that have ignored the role of radiative loss and only focused on drag loss [22–24].

In all calculations above, radiative loss is stimulated by transverse momentum diffusion experienced by the heavy quark or radiated gluon, which, in some cases, is quantified by the jet transport coefficient $\hat{q}$ [25,26]. The drag loss is quantified using the drag coefficient referred to as dE/dx (energy loss per unit distance) or $\hat{e}$ [27].

To the best of our knowledge, no calculation of heavy flavor energy loss has explored the possibility that the drag coefficient $\hat{e}$ (or the longitudinal diffusion coefficient $\hat{e}_2$) may lead to an additional source of radiative loss, beyond that provided by $\hat{q}$. This possibility is immediately clear in the higher twist framework, where the drag (and longitudinal diffusion) coefficient $\hat{e}$ ($\hat{e}_2$) has the boost invariant definition as the loss of light-cone momentum (fluctuation in light-cone momentum) per unit light-cone length (assuming a parton moving in the negative light-cone direction),

$$\hat{e} = \frac{d\langle \Delta p^- \rangle}{dL^-}, \quad \hat{e}_2 = \frac{d\langle \Delta p^{-2} \rangle}{dL^-}. \tag{1}$$

While such transport coefficients lead to little change in the off-shellness of a near on-shell *massless* quark [27,28], they have a considerable impact on the off-shellness of a near on-shell *massive* quark, as discussed in next section. We will demonstrate that, such a term will *only* have an effect on the radiative loss of a patron where the momentum p is comparable to the mass M. Thus for light flavors, and for energetic heavy quarks where, $p \gg M$, this term will have a minimal effect. This was explicitly explored for photon radiation from a light quark in Ref. [29]. We point out that such an effect is by no means limited to the higher-twist scheme, but affects several other formalisms that have considered the radiative loss from a heavy quark in a quark gluon plasma [30–32].

In this paper, we will explore the modification to the calculation of radiative loss, due to the presence of this additional source within the higher twist formalism. To delineate the importance of these terms, we will use power-counting

techniques borrowed from soft collinear effective theory (SCET) [33–36] to identify the regime where these mass dependent terms will cause detectable effects on the gluon bremsstrahlung spectrum. As a first attempt, we will consider only the case of single scattering and single emission. Arguments presented in subsequent sections will demonstrate this to be the leading contribution, given the short formation time of the radiated gluons. In this paper, the analytical expressions for the $\hat{e}$ ($\hat{q}$ and $\hat{e}_2$) induced gluon radiation spectrum will be derived. Numerical calculations for the suppression of B and D mesons, as well as the suppression and azimuthal anisotropy of nonphotonic leptons from the decay of these mesons at LHC and RHIC energies, and comparisons with experimental data will be carried out in a subsequent effort.

The article is organized as follows: In Sec. II, we will setup the basic formalism of deep inelastic scattering (DIS) on a large nucleus, where the hard virtual photon strikes a heavy quark, assumed to be produced in a rare high Q^2 fluctuation inside a proton. In Sec. III, we will carry out diagrammatic studies on the induced gluon radiation off the heavy quark in this system, within the higher twist formalism. We will present and discuss final expressions for gluon bremsstrahlung from such a heavy quark, containing both $\hat{q}$, $\hat{e}$ and $\hat{e}_2$ in Sec. IV. We offer concluding discussions and an outlook in Sec. V. Involved expressions for a set of diagrams are contained in the Appendix.

II. DEEP INELASTIC SCATTERING AND THE SEMIHARD HEAVY QUARK

The setup is based on the deep-inelastic scattering of a virtual photon off a heavy quark within a large nucleus with mass number A. We will study the case where the hard virtual photon scatters with the hard heavy quark converting it to slow moving heavy quark (this is defined below). The propagation of the heavy quark will be factorized from the hard scattering vertex which produces the outgoing slow moving heavy quark. The nucleus has a momentum $P = pA$, where p is the average momentum of a nucleon in this nucleus. In the Breit frame, the exchanged virtual photon possesses no transverse momentum,

$$q \equiv [q^+,q^-,q_\perp] = [q^+,q^-,0]. \tag{2}$$

The process under consideration is the following:

$$e(L_1) + A(P) \to e(L_2) + J_{\mathcal{Q}}(L_{\mathcal{Q}}) + X. \tag{3}$$

In the above process, $e(L_1)$ and $e(L_2)$ represent the incoming and outgoing electrons with momentum L_1 and L_2 respectively. The factor $A(P)$ represents the incoming nucleus with momentum P. The factor $J_{\mathcal{Q}}(L_{\mathcal{Q}})$ is the outgoing jet which contains one heavy quark $\mathcal{Q}$. Due to the absence of valence heavy quarks within the nucleon, the photon will have to strike a heavy quark from a $\mathcal{Q}\bar{\mathcal{Q}}$ fluctuation within the sea of partons. Alternatively one may consider the case of a J/ψ or Υ state bound within a large nucleus, being struck by the hard virtual photon. More detailed discussions on the production of heavy quarks can be found in Ref. [37].

In this work, we will not discuss the production of the heavy quark further. For the purposes of this calculation, this is now contained within a parton distribution function. In essence, by this mechanism a semihard heavy quark has been produced. In what follows, we will focus on the power counting of the momentum components and the modification of the final state. Similar to Ref. [37], we will consider a quark mass $M \gg \Lambda_{\rm QCD}$ and a final outgoing quark momentum which is larger, but of the order of the quark mass.

A. Production of a semihard heavy quark

At the outset we assume that quark-antiquark fluctuations possess minimal momentum (they are almost at rest) in the rest frame of the nucleus. Therefore momentum components of the quark (or the anti-quark) scales as $(p^+_{\mathcal{Q}}, p^-_{\mathcal{Q}}, p_{\mathcal{Q}\perp}) \sim (M/\sqrt{2}, M/\sqrt{2}, 0)$ in the rest frame of the nucleus. Now in a frame where the nucleus is boosted by a large boost factor γ in the "+" direction, momentum components of the heavy quark will scale as

$$p_{\mathcal{Q}} = [p^+_{\mathcal{Q}}, p^-_{\mathcal{Q}}, p_{\mathcal{Q}\perp}] \equiv \left[\gamma\frac{M}{\sqrt{2}}, \frac{1}{\gamma}\frac{M}{\sqrt{2}}, 0\right]. \tag{4}$$

It is important to note that the boost factor γ carries no extra information other than the fact that $p^+_{\mathcal{Q}}$ is very large compared to $p^-_{\mathcal{Q}}$ and hence it is moving fast in the "+" light-cone direction. We select events where the virtual photon strikes this fast moving on-shell quark or antiquark and converts it into a heavy on-shell fermion traveling in the "−" light-cone direction. We further stipulate that this backward propagating heavy fermion be semihard, i.e., the magnitude of its three-momentum is of the order of its mass. This enforces the momentum components of the virtual photon to be

$$q = \left[-\gamma\frac{M}{\sqrt{2}} + \frac{M^2}{2q^-}, q^- - \frac{1}{\gamma}\frac{M}{\sqrt{2}}, 0\right]. \tag{5}$$

This rather cumbersome form arises out of the need to produce a semihard (or slow moving) heavy fermion, after a collision with a hard (or fast moving) fermion. Yet another reason, is to keep the heavy-quark mass as explicit in as many momentum terms as possible. After scattering with this photon, the outgoing quark propagates through the nucleus, with a larger momentum in the "−" light-cone direction. The momentum components of the final state quark are

$$p_f = p_{\mathcal{Q}} + q = \left[\frac{M^2}{2q^-}, q^-, 0\right]. \tag{6}$$

where we assume $q^- \gtrsim M$. Given a large boost factor (γ), one can assume that $\gamma M \gg M \sim q^- \gg M/\gamma$. Hence, we define the hard scale Q as $Q^2 = -q^2 \simeq \gamma M q^-/\sqrt{2}$. We consider $M \sim q^- \sim \sqrt{\lambda}Q$ where $\lambda \sim 1/\gamma$ for this "semihard" heavy quark. The term "semihard" defines a quark whose momentum is not an order of magnitude larger than its mass. It is also important to articulate at this point that γ is not the boost factor of the semihard quark (moving in "−" light-cone direction) but it is that for the very fast moving initial hard quark (moving in the "+" light-cone direction) before the scattering takes place. Numerically the boost factor could be $\gtrsim$100 (hence $\lambda \lesssim 0.1$).

B. Power counting and the small λ parameter

In order to set up the power counting, in this study, we have introduced the dimensionless small parameter λ. Power corrections to hard process are generally suppressed by factors of a hard scale, $Q^2 \gg \Lambda_{\rm QCD}$. The introduction of the parameter λ, to represent semihard scales as λQ and softer scales as $\lambda^2 Q$, is a concept borrowed from soft collinear effective theory (SCET) [38,39]. In what follows, we will retain leading and next-to-leading terms in λ power counting, neglecting all terms which scale with λ^2 or a higher power of λ [40]. We have chosen the scaling variable λ in such a way that perturbation theory may be applied down to momentum transfer scales at or above $\lambda^{3/2} Q \sim \Lambda_{\rm QCD}$. In our study,

$$\lambda^0 \gg \sqrt{\lambda} \gg \lambda \gg \lambda^{\frac{3}{2}}. \tag{7}$$

Based on the power counting setup and the choice of incoming and outgoing quark momentum, we can outline several important scales in the problem of a heavy quark propagating through the nuclear medium, scattering off constituents in the medium, and emitting real gluons. We remind the reader that given the semihard momentum of the heavy quark, collinear emission is suppressed due to the mass of the heavy quark, i.e., the *dead cone* effect [41].

In the subsequent section, the calculation of the process of single scattering and single emission from a heavy quark will be carried out. Here we outline the power counting (in λ) of the relevant momentum components that will arise in the calculation. The virtuality of the hard photon defines the hardest scale in the problem, Q, similar to the case of light quark production in DIS. The incoming or initial heavy quark has momentum components $p_i(p_i^+, p_i^-, p_{i\perp}) \sim (\lambda^{-\frac{1}{2}}, \lambda^{\frac{3}{2}}, 0)Q$, the outgoing heavy quark has momentum components $p_f(p_f^+, p_f^-, p_{f\perp}) \sim (\sqrt{\lambda}, \sqrt{\lambda}, 0)Q$. It is customary to mention that the above scales signify only the order of magnitudes and not the actual value of the momentum components. For outgoing heavy quark, the z component of the momentum is $p_{f,z} = (p_f^+ - p_f^-)/\sqrt{2} \sim O(\sqrt{\lambda}) - O(\sqrt{\lambda}) \sim O(\sqrt{\lambda})$ Also the mass of the semihard heavy quark scales as $M \sim \sqrt{\lambda} Q$. This choice of incoming parton and photon momenta scales (not actual value) ensures that the momentum of the final outgoing heavy quark is of the order of its mass, as discussed in the previous subsection. In what follows, we will demonstrate that the leading contribution to gluon emission arises from the region where real emitted gluons have momenta which scale as $l \sim (\lambda, \lambda, \lambda)Q$. This also ensures that both the z component of the momentum, $l_z = (l^+ - l^-)/\sqrt{2} \sim O(\lambda) - O(\lambda) \sim O(\lambda)$, as well as the transverse momentum are $\sim O(\lambda)$. The fraction of light-cone momenta carried out by the gluon is $y = l^-/p^- \sim \sqrt{\lambda}$. Also somewhat different from the case of light flavors is the scaling of the virtual Glauber gluons: $k \sim (\lambda^{\frac{3}{2}}, \lambda^{\frac{3}{2}}, \lambda)Q$ with $k^2 = 2k^+k^- - k_\perp^2 \simeq -k_\perp^2$. As we will demonstrate below, these choices of momentum scales tend to enhance the gluon emission rate.

There is another consequence of this choice of scales which relates to how the single gluon emission kernel may be iterated. Unlike the case for light flavors, the formation length of a gluon

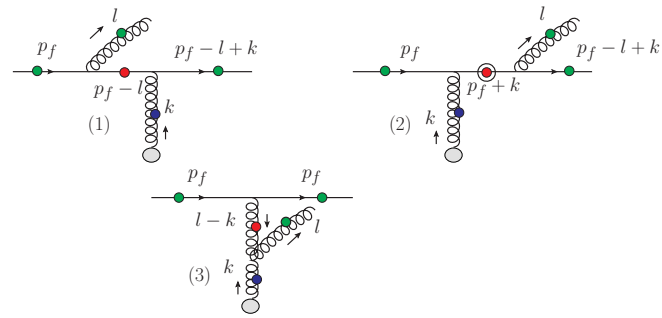

FIG. 1. Gluon bremsstrahlung by heavy quark. External legs with green blobs are on shell, while off-shell internal legs have either a red blob or a blue blob. Lines with blue blobs are in-medium Glauber gluons. Red and blue blobs with (without) an additional dark ring indicate spacelike (timelike) off shell.

with momentum components $l \sim (\lambda, \lambda, \lambda)Q$ is

$$\tau_Q = \frac{2l^-}{l_\perp^2} \sim \frac{1}{\lambda Q}, \tag{8}$$

which is rather short compared to the formation length of $\tau_q \sim 1/\lambda^2 Q$ for gluon radiation from near on-shell light flavors. This indicates that there cannot be many scatterings per emission. As a result, in what follows, we derive the single scattering per gluon emission rate. This single gluon emission kernel, induced by single scattering, will have to be iterated to obtain the full energy loss of a semihard heavy quark.

Many readers may find the presence of factors of $\sqrt{\lambda}$ somewhat disconcerting. We could have simply replaced this with a new λ. We refrain from defining a new dimensionless parameter λ, so as to make contact with prior definitions of λ used in the case of light quarks, where λQ represented the transverse momentum of the radiated gluons from a hard parton, or the transverse momentum from scattering of a gluon in the medium. Thus, to continue to draw a parallel with the prior results from light flavor energy loss, we require $\lambda Q \sim 1$ GeV.

To get a physical feel of these scaling relations, one may typically assume $Q \sim 100\,\text{GeV}, \sqrt{\lambda} Q \sim 10\,\text{GeV}, \lambda Q \sim 1\,\text{GeV}, \lambda^{\frac{3}{2}} Q \sim \Lambda_{\rm QCD}$. We will retain terms that are $O(\sqrt{\lambda})$ suppressed compared to the leading terms, but we ignore all terms that are suppressed by $O(\lambda)$ and higher. Thus, terms with $M^2/Q^2 \sim \lambda$ will eventually be ignored.

C. Effects on off-shell internal legs

A schematic diagram for single gluon (of momentum l) bremsstrahlung by an on-shell heavy quark (of momentum p_f) is given in Fig. 1. Any external legs with a green blob are on shell, while off-shell internal legs have either a red blob or a blue blob. Lines with blue blobs are in-medium Glauber gluons with momentum k. In order to see the effect of non-negligible k^- of the medium gluons one may want to calculate the off-shellness or virtuality of the internal lines (with a red blob). In terms of the variables defined in Eq. (18)

virtualities of the the off-shell internal lines are as follows;

$$D_1 = (p_f - l)^2 - M^2 = 2P^+q^-(1-y)\left[-x_B + x_0 - x_L - \frac{x_M}{1-y}\right], \tag{9}$$

$$D_2 = (p_f + k)^2 - M^2 = 2P^+q^-(1+y\eta)\left[-x_B + x_0 + x_1 - \frac{x_M}{(1+y\eta)} - \frac{x_K}{(1+y\eta)}\right], \tag{10}$$

$$D_3 = (l-k)^2 = 2P^+q^-y(1-\eta)\left[-x_1 - \frac{1-y}{y(1-\eta)}x_D - \frac{\eta(1-y)}{(1-\eta)}x_L\right]. \tag{11}$$

If one imposes the condition that the final outgoing quark is also on shell, i.e., $(p_f - l + k)^2 - M^2 = 0$, one is left with

$$D_1 = (p_f - l)^2 - M^2 = -\frac{1}{y}[l_\perp^2 + y^2M^2], \tag{12}$$

$$D_2 = (p_f + k)^2 - M^2 = +\frac{1}{y}\left(1 - y + \frac{k^-}{q^-}\right)^{-1}\left[\left\{\left(1 + \frac{k^-}{q^-}\right)l_\perp - yk_\perp\right\}^2 + y^2M^2\right], \tag{13}$$

$$D_3 = (l-k)^2 = -\left(1 - y + \frac{k^-}{q^-}\right)^{-1}\left[(l_\perp - k_\perp)^2 + y^2M^2\left(1 - \frac{k^-}{l^-}\right)^2\right]. \tag{14}$$

In the above expressions k^- appears either as $k^-/q^- \sim O(\lambda)$ or as $k^-/l^- \sim O(\sqrt{\lambda})$. While the former can be neglected, one needs to retain k^-/l^- as it is $O(\sqrt{\lambda})$. We also notice that this term appears only in D_3, i.e., in the three-gluon vertex diagram and also attached with the mass term of D_3. It clearly shows that the leading mass effect due to non-negligible k^- appears for heavy quarks and not for light quarks. Hence the transport coefficient associated with k^- leads to little change in the off-shellness of a near on-shell *massless* quark; it has a considerable impact on the off-shellness of a near on-shell *massive* quark, as mentioned in the Introduction.

III. INDUCED GLUON RADIATION OFF THE HEAVY QUARK

In this section we will discuss some contributions to the next-to-leading order correction to semi-inclusive DIS on a large nucleus with a quark and gluon in the final state. By next-to-leading order, we simply mean including one interaction term in the amplitude and complex conjugate, which converts a single quark to a quark and a gluon. The diagrams we will consider will also contain two scatterings for the full cross section, with both scatterings in the amplitude, both in the complex conjugate, or one in amplitude and one in complex conjugate. The double differential cross section for the semi-inclusive process of an electron with incoming momentum L_1 and outgoing momentum L_2, undergoing DIS off a nucleus (with momentum pA), leading to the production of a final state heavy quark with transverse momentum $l_{Q_\perp}$ and a final state gluon with transverse momentum $l_\perp \gg \Lambda_{\rm QCD}$, may be expressed as

$$\frac{E_{L_2}d\sigma}{d^3L_2d^2l_{Q_\perp}d^2l_\perp dy} = \frac{\alpha_{em}^2}{2\pi sQ^4}L_{\mu\nu}\frac{dW^{\mu\nu}}{d^2l_{Q_\perp}d^2l_\perp dy}. \tag{15}$$

In the equation above, $s = (p + L_1)^2$ is the total invariant mass of the lepton nucleon system. In the single photon exchange approximation, the leptonic part of the cross section is easily expressed in terms of the leptonic tensor denoted as $L^{\mu\nu}$, given as

$$L_{\mu\nu} = \tfrac{1}{2}\mathrm{Tr}[\not{L}_1\gamma_\mu\not{L}_2\gamma_\nu]. \tag{16}$$

In what follows, the focus will lie entirely on the hadronic tensor $W^{\mu\nu}$. We will carry out calculations of a set of contributions to $W^{\mu\nu}$ at next-to-leading order (NLO) as described above, and next-to-leading twist (NLT), meaning double scattering in the cross section.

Already, at NLO and NLT, there are several interfering diagrams to consider. In this section, the calculation of one of the diagrams that contributes to single scattering induced single gluon emission will be carried out in some detail to familiarize the reader with the approximations carried out in this article. Figure 2 represents the diagram that will be evaluated. This diagram corresponds to the process where a semihard heavy quark produced after DIS radiates a gluon followed by a scattering in the medium, and finally exits the nucleus.

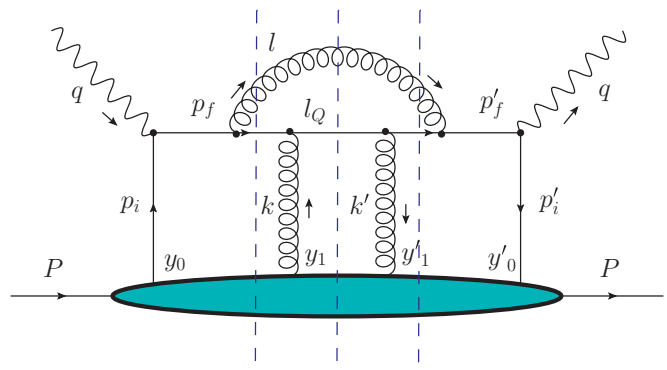

FIG. 2. A representative single gluon emission diagram, where gluon emission is induced by single scattering. This is a symmetric diagram with scattering off the final produced quark. Three separate cuts, denoted as central, left, and right are indicated by the dashed lines.

In this study, calculations will be carried out in axial gauge, $n \cdot A = 0$, with $n \equiv (1,0,0_\perp)$ and $A^- = 0$. In $A^- = 0$ gauge, the double scattering of a quark radiating a gluon contains a total of nine central cut diagrams where the cut line lies between the two scatterings. It also contains seven left cut diagrams and seven right cut diagrams. In this section, the central cut diagram of Fig. 2 will be analyzed in detail.

In this section and what follows, only the real contribution where the radiated gluon line has been cut will be considered. The entire contribution from virtual diagrams, which contain a quark gluon fluctuation either in the amplitude or complex conjugate, could be obtained using unitary conservation methods as outlined in Ref. [42].

This NLO-NLT contribution to the hadronic tensor may be expressed as

$$W^{\mu\nu} = g^4(-g_\perp^{\mu\nu}) \int \frac{d^4y_0' d^4p_i'}{(2\pi)^4} \frac{d^4y_1' d^4k'}{(2\pi)^4} \frac{d^4y_1 d^4k}{(2\pi)^4} \frac{d^4y_0 d^4p_i}{(2\pi)^4} \frac{d^4l}{(2\pi)^4} \frac{d^4l_Q}{(2\pi)^4} e^{ip_i' y_0'} e^{ik' y_1'} e^{-iky_1} e^{-ip_i y_0}$$
$$\times \mathrm{Tr}\left[\frac{1}{2}\gamma^- \frac{-i(\not{p}_f + M)}{p_f^2 - M^2 - i\epsilon} \gamma_\alpha \frac{-i(\not{p}_f - \not{l} + M)}{(p_f - l)^2 - M^2 - i\epsilon} \not{l}_q G^{\alpha\beta} \frac{i(\not{p}_f - \not{l} + M)}{(p_f - l)^2 - M^2 + i\epsilon} \gamma_\beta \frac{i(\not{p}_f - \not{l} + M)}{(p_f - l)^2 - M^2 + i\epsilon} \right]$$
$$\times 2\pi\delta(l^2) 2\pi\delta\left(l_Q^2 - M^2\right)(-iT^a)(iT^a)\langle A|\bar{\psi}(y_0')\gamma^+ A^+(y_1')A^+(y_1)\psi(y_0)|A\rangle. \tag{17}$$

We have defined the following momentum fractions for convenience:

$$y = \frac{l^-}{q^-}, \quad \eta = \frac{k^-}{l^-}, \quad x_B = \frac{Q^2}{2P^+q^-}$$
$$x_0 = \frac{p_i^+}{P^+}, \quad x_1 = \frac{k^+}{P^+}, \quad \chi = \frac{y^2M^2}{l_\perp^2}, \quad \zeta = \frac{1-y}{1-y+\eta y},$$
$$x_L = \frac{l_\perp^2}{2P^+q^-y(1-y)}, \quad x_D = \frac{k_\perp^2 - 2l_\perp k_\perp}{2P^+q^-},$$
$$x_K = \frac{k_\perp^2}{2P^+q^-}, \quad \kappa = \frac{1}{1+(1-y)^2}, \quad x_M = \frac{M^2}{2P^+q^-}. \tag{18}$$

In what follows, we will simplify both numerator and denominator by retaining only leading terms in the λ power counting highlighted above. This is followed by taking the trace in the numerator and contour integrations to simplify the denominator.

The factor $G^{\alpha\beta}$ is the polarization tensor, and in $A^- = 0$ gauge it has the form

$$G^{\alpha\beta} = -g^{\alpha\beta} + \frac{n^\alpha l^\beta + n^\beta l^\alpha}{nl}. \tag{19}$$

The structure of $n \equiv (1,0,0_\perp)$ implies $n \cdot l = l^-$. Within this kinematic set up, in $A^- = 0$ gauge, the leading component of the gluon field is A^+.

The spin sum in the numerator, containing the entire set of γ matrices from the quark propagators, together with those from the interaction with the gauge field, may be partially simplified and expressed as

$$\mathcal{N}_{11}^c = \mathrm{Tr}\Bigg[\frac{1}{2}\gamma^-\Bigg\{\gamma^+q^-\gamma_\mu\frac{n^\mu(l_\perp)^\nu}{l^-}\gamma^+(q^- - l^-) + \gamma_\perp^\alpha p_{f\perp\alpha}\gamma_{\perp\mu}(-g_\perp^{\mu\nu})\gamma^+(q^- - l^-)$$
$$+\gamma^+q^-\gamma_{\perp\mu}(-g_\perp^{\mu\nu})\gamma_\perp^\alpha(p_{f\perp} - l_\perp)_\alpha\Bigg\}\gamma^-\gamma^+(q^- - l^- + k^-)\gamma^-\Bigg\{\gamma^+(q^- - l^-)\gamma_\rho\frac{n^\rho(l_\perp)_\nu}{l^-}\gamma^+q^-$$
$$+\gamma^+(q^- - l^-)\gamma_\perp^\rho(-g_\perp)_{\rho\nu}\gamma_\perp^\beta p_{f\perp\beta} + \gamma_\perp^\beta(p_{f\perp} - l_\perp)_\beta\gamma_\perp^\rho(-g_\perp)_{\rho\nu}\gamma^+q^-\Bigg\}\Bigg]$$
$$+\mathrm{Tr}\Bigg[\frac{1}{2}\gamma^-\{M\gamma_{\perp\mu}(-g_\perp^{\mu\nu})\gamma^+(q^- - l^-) + \gamma^+q^-\gamma_{\perp\mu}(-g_\perp^{\mu\nu})M\}$$
$$\times\gamma^-\gamma^+(q^- - l^- + k^-)\gamma^-\{\gamma^+(q^- - l^-)\gamma_\perp^\rho(-g_\perp)_{\rho\nu}M + M\gamma_\perp^\rho(-g_\perp)_{\rho\nu}\gamma^+q^-\}\Bigg]. \tag{20}$$

Note that terms containing $\gamma^- p_f^+$ never contribute to the trace because there is always an adjacent factor of γ^-, and $\gamma^-\gamma^- = \gamma^+\gamma^+ = 0$. One may evaluate the trace: using the relation $\gamma^+\gamma^- = 2 - \gamma^-\gamma^+$, Eq. (20) simplifies to

$$\mathcal{N}_{11}^c = \frac{2(2q^-)^3}{y}(1 - y + y\eta)[P(y)l_\perp^2 + y^4M^2]. \tag{21}$$

Note that the mass independent portion contains the standard vacuum splitting function $P(y)$ while the mass dependent part has a separate dependence on the momentum fraction of the radiated gluon (y). In the soft emission kinematic limit where $y \ll 1$, one may neglect the mass term. However, in this work we will retain it throughout.

The set of denominators can now be evaluated using contour integration. For the central cut diagram of Fig. 2, this yields the phase factor

$$\bar{I}^{c}_{11} = \exp\left[i\left(x_B + x_L + \frac{x_M}{1-y}\right)P^+(y_0'^- - y_0^-)\right]\exp\left[i\left(\zeta x_D + (\zeta-1)\frac{x_M}{1-y} - \zeta\frac{\eta y^2}{1-y}x_L\right)P^+(y_1'^- - y_1^-)\right]$$
$$\times\theta(y_1^- - y_0^-)\theta(y_1'^- - y_0'^-)$$
$$\times\left\{1 - \exp\left[-i\left(x_L + \frac{y}{1-y}x_M\right)P^+\left(y_1^- - y_0^-\right)\right]\right\}\left\{1 - \exp\left[i\left(x_L + \frac{y}{1-y}x_M\right)P^+(y_1'^- - y_0'^-)\right]\right\}.$$

This single diagram contains four contributions depending on the one propagator that remains off shell after contour integration.

Multiplying through we find four terms similar to the work of Ref. [42] [Eqs. (A20)–(A23)]. The first term where the same propagator is off shell in both amplitude and complex conjugate corresponds to the so-called hard-soft process (this is terminology used and described by the authors of Ref. [42], in Sec. III of that paper), where the gluon radiation is induced by the initial hard scattering. The heavy quark is knocked off-shell by the initial hard scattering and becomes on-shell after radiating the on-shell gluon. Afterwards, the on-shell quark or gluon will have a scattering with another soft medium gluon from the nucleus. The second term is the case where the quark is on-shell immediately after the first hard scattering. Gluon radiation is induced by subsequent scattering of the heavy quark off a in-medium gluon which carries a specific finite momentum fraction. This is often referred to as "hard-hard" scattering (terminology used and described by the authors of Ref. [37], in Sec. III of that paper). The two cross terms, where different propagators are off shell in the amplitude and complex conjugate, represent interference between soft-hard and hard-hard scatterings.

The equations derived above contain both longitudinal and transverse momentum exchanges with the medium. The portion due to transverse exchange may be isolated by imposing that $k^- \to 0 (\eta \to 0, \zeta \to 1)$ limit, and then comparing with expressions from similar diagrams in Ref [21]. One will immediately note that factors containing x_M which contribute to the Landau-Pomeranchuck-Migdal (LPM) [43,44] effect are not modified by factors of k^-, while factors containing x_D are modified by the presence of k^-. Factors of x_D will eventually be absorbed in the definition of the transport coefficients including $\hat{q}$. Such factors introduce a nontrivial dependence of in-medium transport coefficients on the mass of the probe.

In this section, we have demonstrated how a certain diagram for heavy-quark production and energy loss via gluon radiation can be simplified. Similar rules will be applied to all other real diagrams which include a cut of the radiated gluon line. In the subsequent section, all real diagrams will be combined to obtain the real gluon emission spectrum from a heavy quark that undergoes one scattering and one emission after production.

IV. GLUON EMISSION SPECTRUM

In the preceding section we evaluated the diagram in Fig. 2, in some detail, to highlight the approximations that will be made in the course of the full calculation. In this section, the result of the sum of all real diagrams (with an emitted gluon in the final state), will be presented. This will be followed by a gradient expansion in the exchanged transverse momentum ($k_\perp \to 0$). While the leading term in the limit of $k_\perp \to 0$, will correspond to a gauge correction to the vacuum process of gluon radiation from a heavy quark, the focus in this section will be on first correction in the $k_\perp \to 0$ limit, usually denoted as the next-to-leading twist contribution.

In total, there are 11 separate topologically distinct diagrams similar to that in Fig. 2. We denote these with two subscripts: $m,n = 1,\ldots,3$, where, m denotes the location of the scattering in the amplitude, and n denotes the location in the complex conjugate, for the case of a central cut, where one gluon scattering is on either side of the cut line. In either case of m or n, 1 signifies that the scattering occurs on the quark line beyond emission, 2 signifies scattering on the quark line between the hard production and the emission, and 3 signifies scattering of the emitted gluon. Each one of these diagrams will also generate a left and right cut component, where the cut line will be moved to the left or right of the scatterings, with the topology of the diagram held fixed. There are also the two special configurations, where both scatterings occur between the hard production and the gluon emission in the amplitude or complex-conjugate. These are denoted as $\mathcal{C}_{0,1}$ and $\mathcal{C}_{1,0}$. The next-to-leading twist portion, of the sum over all possible cuts, for each of these contributions is outlined in the Appendix.

Adding all the contributions from all the diagrams, categorized in the Appendix, we obtain the entire contribution to the hadronic tensor. In what follows, we decompose the hadronic tensor as

$$W^{\mu\nu} = g^4 2\pi(-g_\perp^{\mu\nu})\mathcal{H}^{c,l,r}. \tag{22}$$

The entire contribution from all real diagrams is contained in the factor $\mathcal{H}^{c,l,r}$. This includes the initial hard scattering, the final state scattering of the quark or gluon, and the emission vertex. Virtual contributions, where the final state radiated gluon is not cut, will not be considered in this effort. Some part of the spin sum in the numerator has already been factorized out in the term $-g_\perp^{\mu\nu}$ above. In what follows, we will simplify $\mathcal{H}^{c,l,r}$ by factoring different contributions within it and then applying approximations to them separately. In the interest of readability, the exact details of the calculation for each diagram separately are included in the Appendix.

This entire factor $\mathcal{H}^{c,l,r}$ is obtained as

$$\begin{aligned}\mathcal{H}^{c,l,r} &= \sum_{m,n=1}^{3} \mathcal{C}^{c,l,r}_{m,n} + \mathcal{C}_{0,1} + \mathcal{C}_{1,0} \\ &= \frac{2\pi\alpha_s}{N_c}\int dl_\perp^2 H^{c,l,r} \\ &\quad\times \exp\left[i\left(x_B + x_L + \frac{x_M}{1-y}\right)P^+(y_0'^- - y_0^-)\right. \\ &\quad + i\left(\zeta x_D + (\zeta-1)\frac{x_M}{1-y} - \zeta\frac{\eta y^2}{1-y}x_L\right) \\ &\quad\left.\times P^+(y_1'^- - y_1^-)\right] \\ &\quad\times\langle A|\bar\psi(y_0')\gamma^+A^+(y_1')A^+(y_1)\psi(y_0)|A\rangle. \end{aligned} \tag{23}$$

In the equation above, cut-specific phase factors and the hard part for each cut are entirely contained within $H^{c,l,r}$. The overall phase factor represents the generic portion of the phase factor.

In order to calculate the next-to-leading power contribution to the semi-inclusive hard partonic cross section, one needs to expand the cross section in $k_\perp$ and in k^-. In each case, we will extract the corresponding transport coefficients inside the gluon emission spectrum kernel for the semihard heavy quark [45]. Factors of $k_\perp$ and k^- are absorbed as derivatives within the definition of the transport coefficients [e.g., $k_\perp A^+(\vec y_\perp)\exp(i\vec k_\perp\cdot\vec y_\perp) = -i\nabla_\perp A^+(\vec y_\perp)\exp(i\vec k_\perp\cdot\vec y_\perp) \simeq iF^{+\perp}(\vec y_\perp)\exp(i\vec k_\perp\cdot\vec y_\perp)$].

We will also factor the four-point non-perturbative operator using the usual phenomenological factorization, which for the case of transverse scattering may be expressed as

$$\begin{aligned}&\langle A|\bar\psi(y_0')\gamma^+F_\perp^+(y_1')F_\perp^+(y_1)\psi(y_0)|A\rangle \\ &\quad\simeq C_p^A\langle p|\bar\psi(y_0')\gamma^+\psi(y_0)|p\rangle\frac{\rho}{2p^+}\langle p|F_\perp^+(y_1')F_\perp^+(y_1)|p\rangle. \end{aligned} \tag{24}$$

The first operator product on the right hand side of the equation above will yield the incoming quark distribution function within one nucleon. The second operator product will yield the transport coefficient due to the scattering of the final state, off a gluon within a nucleon in the nucleus. We have assumed the average condition that both nucleons have a momentum $p = P/A$. The factor ρ represents the nucleon density within the nucleus, and C_p^A represents an overall normalization constant that contains the nucleon density. The factor of $\rho/(2p^+)$ is written separately, as that will be absorbed within the definition of the transport coefficient.

These transport coefficients, defined below, are nonperturbative objects, which are factorized from the hard part that describes the propagation of the heavy quark. While the exact value of each of these coefficients depends on the nonperturbative dynamics of the medium, the relative contributions of the different hard parts that appear as a multiplicative factor along with these coefficients will be calculated below. Terms for the transverse diffusion $\hat q$ and the drag (and longitudinal diffusion) coefficient $\hat e$ ($\hat e_2$) can be obtained through derivatives of the kernel with respect to the transverse and "−" light-cone component of the exchange momentum,

$$\begin{aligned}&\left[\nabla^2_{k_\perp},\nabla_{k^-},\nabla^2_{k^-}\right]H^{c,l,r}\big|_{k_\perp,k^-=0} \\ &\quad= 4C_A\left(\frac{1+(1-y)^2}{y}\right)\frac{l_\perp^4}{[l_\perp^2+y^2M^2]^4}\tilde H^{\hat q,\hat e,\hat e_2}_{c,l,r}. \end{aligned} \tag{25}$$

In the equation above, the factor $\tilde H^{\hat q,\hat e,\hat e_2}_{c,l,r}$ represents several terms, depending on the cut taken, i.e., central c, left l, or right r, and the momentum component with respect to which the Taylor expansion is carried out, i.e., $\hat q$ for the second derivative in terms of $k_\perp$, $\hat e$ for the first derivative with respect to k^-, and $\hat e_2$ for the second derivative with respect to k^-. One should note that, for each case, once the derivatives have been taken, both factors of the momentum $k_\perp$,k^- are set to zero. The complete expressions for $\tilde H^{\hat q,\hat e,\hat e_2}_{c,l,r}$ can be expressed as a sum of products of a phase factor and a nonphase factor coefficient, expressed as $c_n^{\hat q,\hat e,\hat e_2}$:

$$\begin{aligned}\tilde H_c^{\hat q,\hat e,\hat e_2} &= c_1^{\hat q,\hat e,\hat e_2}\left[1-e^{-i(x_L+\frac{y}{1-y}x_M)P^+(y_1^- - y_0^-)}\right]\left[1-e^{i(x_L+\frac{y}{1-y}x_M)P^+(y_1'^- - y_0'^-)}\right] + c_2^{\hat q,\hat e,\hat e_2}\left\{e^{-i(x_L+\frac{y}{1-y}x_M)P^+(y_1^- - y_0^-)}\right. \\ &\quad\times\left[1-e^{i(x_L+\frac{y}{1-y}x_M)P^+(y_1'^- - y_0'^-)}\right] + \left[1-e^{-i(x_L+\frac{y}{1-y}x_M)P^+(y_1^- - y_0^-)}\right]\left.e^{i(x_L+\frac{y}{1-y}x_M)P^+(y_1'^- - y_0'^-)}\right\} \\ &\quad + c_3^{\hat q,\hat e,\hat e_2}\left[e^{-i(x_L+\frac{y}{1-y}x_M)P^+(y_1^- - y_0^-)}\right]\left[e^{i(x_L+\frac{y}{1-y}x_M)P^+(y_1'^- - y_0'^-)}\right], \\ \tilde H_l^{\hat q,\hat e,\hat e_2} &= c_4^{\hat q,\hat e,\hat e_2}\left[e^{-i(x_L+\frac{y}{1-y}x_M)P^+(y_0'^- - y_1'^-)} - e^{-i(x_L+\frac{y}{1-y}x_M)P^+(y_0'^- - y_1^-)}\right] + c_5^{\hat q,\hat e,\hat e_2}\left[1-e^{-i(x_L+\frac{y}{1-y}x_M)P^+(y_0'^- - y_1'^-)}\right], \\ \tilde H_r^{\hat q,\hat e,\hat e_2} &= c_4^{\hat q,\hat e,\hat e_2}\left[e^{-i(x_L+\frac{y}{1-y}x_M)P^+(y_0^- - y_1^-)} - e^{-i(x_L+\frac{y}{1-y}x_M)P^+(y_0^- - y_1'^-)}\right] + c_5^{\hat q,\hat e,\hat e_2}\left[1-e^{-i(x_L+\frac{y}{1-y}x_M)P^+(y_0^- - y_1^-)}\right]. \end{aligned}$$

In each case above, the coefficients $c_n^{\hat q,\hat e,\hat e_2}$ depend on the momentum component being considered. The subscript n merely denotes the order in which the coefficient occurs: c_1, c_2 and c_3 appear in the expression for the central cut, where c_4 and c_5 appear in both the left and right cuts. We list them in the following for each different case, starting from the case of transverse diffusion, i.e., $\hat q$.

The coefficients are

$$
\begin{aligned}
c_1^{\hat{q}} &= 1-(2-3\kappa y^2)\chi+(1-\kappa y^2)\chi^2,\\
c_2^{\hat{q}} &= -\frac{y}{2}+\left[\left(1-\frac{1}{2}\kappa y^2-\kappa y^3\right)+y^2\frac{C_F}{C_A}\left(2-\kappa y^2\right)\right]\chi-\left[\frac{1}{2}(y-\kappa y^2)-y^2\frac{C_F}{C_A}(\kappa y^2)\right]\chi^2,\\
c_3^{\hat{q}} &= y^2\frac{C_F}{C_A}[1-4(1-\kappa y^2)\chi+(1-2\kappa y^2)\chi^2],\\
c_4^{\hat{q}} &= \left[1+\frac{y^2}{1+(1-y)^2}\chi\right]\left[\frac{C_F}{C_A}y^2+1-2y\right]\chi,\\
c_5^{\hat{q}} &= \left[1+\frac{y^2}{1+(1-y)^2}\chi\right]\chi.
\end{aligned}
\tag{26}
$$

The momentum fractions y, κ, and χ are defined in Eq. (18). For the longitudinal drag coefficient $\hat{e}$, the c factors are

$$
c_1^{\hat{e}}=\frac{y^2M^2}{l^-}\left[\frac{1}{2}+\frac{1}{2}(1+\kappa y^2)\chi+\frac{1}{2}\chi^2\right],\quad c_2^{\hat{e}}=\frac{y^2M^2}{l^-}\left[-\frac{1}{4}-\frac{1}{4}(1+\kappa y^2)y^2\chi-\frac{1}{4}\chi^2\right],\quad c_3^{\hat{e}}=0,\quad c_4^{\hat{e}}=0,\quad c_5^{\hat{e}}=0.
$$

For longitudinal diffusion coefficient $\hat{e}_2$, the c- factors are

$$
\begin{aligned}
c_1^{\hat{e}_2} &= \frac{y^2M^2}{(l^-)^2}\left[-\frac{1}{2}+\left(\frac{7}{2}-\frac{1}{2}\kappa y^2\right)\chi+\frac{7}{2}y^2\chi^2\right],\quad c_2^{\hat{e}_2}=\frac{y^2M^2}{(l^-)^2}\left[\frac{1}{4}-\left(\frac{3}{4}-\frac{1}{4}\kappa y^2\right)\chi-\frac{3}{4}\kappa y^2\chi^2\right],\\
c_3^{\hat{e}_2} &= 0,\quad c_4^{\hat{e}_2}=0,\quad c_5^{\hat{e}_2}=0.
\end{aligned}
$$

All the terms presented above can be combined to obtain the real single gluon emission spectrum. In the second line of the equation below [Eq. (27)], we have retained terms only up to $O(\sqrt{\lambda})$, the approximation that has been justified in this study. All terms which scale as $O(\lambda)$ or greater have been neglected. We express the gluon spectrum per unit light-cone length as

$$
\begin{aligned}
\frac{dN_g}{dy dl_\perp^2 d\tau} &= 2\frac{\alpha}{\pi}P(y)\frac{1}{l_\perp^4}\left(\frac{1}{1+\chi}\right)^4\sin^2\left(\frac{l_\perp^2}{4l^-(1-y)}(1+\chi)\tau\right)\left[\left\{c_1^{\hat{q}}+c_2^{\hat{q}}\right\}\hat{q}+4\left\{c_1^{\hat{e}}+c_2^{\hat{e}}\right\}\hat{e}+2\left\{c_1^{\hat{e}_2}+c_2^{\hat{e}_2}\right\}\hat{e}_2\right]\\
&= 2\frac{\alpha}{\pi}P(y)\frac{1}{l_\perp^4}\left(\frac{1}{1+\chi}\right)^4\sin^2\left(\frac{l_\perp^2}{4l^-(1-y)}(1+\chi)\tau\right)\\
&\quad\times\left[\left\{\left(1-\frac{y}{2}\right)-\chi+\left(1-\frac{y}{2}\right)\chi^2\right\}\hat{q}+\frac{l_\perp^2}{l^-}\chi(1+\chi)^2\hat{e}+\frac{l_\perp^2}{(l^-)^2}\chi\left(\frac{1}{2}-\frac{11}{4}\chi\right)\hat{e}_2\right].
\end{aligned}
\tag{27}
$$

In the equation above, we have defined a mean light-cone location of the first scattering (between the amplitude and complex conjugate) as

$$
\tau=\frac{y_1^-+y_1'^-}{2}. \tag{28}
$$

We also define the offset between the light cone locations in the amplitude and complex conjugate as

$$
y^-=y_1^--y_1'^-. \tag{29}
$$

This variable enters the definitions of all transport coefficients that will be discussed in this paper. There are three transport coefficients, which contain the nonperturbative expectation of the gluon field strength operators: the transverse diffusion coefficient, $\hat{q}$, which represents the transverse momentum squared per unit light-cone length, exchanged between the hard quark and the medium; the longitudinal drag per unit light-cone length, $\hat{e}$, caused due to the exchange of light-cone components of momentum; and $\hat{e}_2$, the diffusion in light-cone momentum, per unit light-cone length:

$$
\begin{aligned}
\hat{q} &= \frac{4\pi^2C_R\alpha_s}{N_C^2-1}\int\frac{dy^-}{\pi}\frac{\rho}{2p^+}\\
&\quad\times\langle A|F_\perp^+(y^-)F^{\perp+}(0)|A\rangle e^{-i\bar{\Delta}P^+y^-},\\
\hat{e} &= \frac{4\pi^2C_R\alpha_s}{N_C^2-1}\int\frac{dy^-}{\pi}\frac{\rho}{2p^+}\\
&\quad\times\langle A|i\partial^-A^+(y^-)A^+(0)|A\rangle e^{-i\bar{\Delta}P^+y^-},\\
\hat{e}_2 &= \frac{4\pi^2C_R\alpha_s}{N_C^2-1}\int\frac{dy^-}{\pi}\frac{\rho}{2p^+}\\
&\quad\times\langle A|F^{-+}(y^-)F^{-+}(0)|A\rangle e^{-i\bar{\Delta}P^+y^-}.
\end{aligned}
\tag{30}
$$

In the equations above, we observe the appearance of another momentum fraction:

$$
\bar{\Delta}=\zeta x_D+(\zeta-1)\frac{x_M}{1-y}-\zeta\frac{\eta y^2}{1-y}x_L. \tag{31}
$$

The presence of such a momentum fraction indicates that the range of momentum fractions in the definition of $\hat{q}$, $\hat{e}$, and $\hat{e}_2$ for heavy-quark scattering is different from that for light flavor energy loss. This indicates that the actual value of $\hat{q}$ (or even $\hat{e}$ or $\hat{e}_2$) for heavy quarks may be different from that for light quarks. Thus, careful analysis of heavy-quark energy loss may lead to an understanding of the x dependence of the in-medium gluon distribution function that sources transport coefficients, and may, in the end, lead to an understanding of the degrees of freedom within dense media, where heavy-quark energy loss is carried out.

V. CONCLUSION AND OUTLOOK

In this work, the gluon bremsstrahlung from a "semihard" heavy quark in a dense nuclear medium has been studied in greater detail than in several earlier efforts. In this work, we have considered a hard virtual photon scattering off a hard heavy quark (within a proton), that converts it to a slowly moving heavy quark that moves through the remainder of the nucleus before escaping and fragmenting into a jet containing a heavy meson.

In this work both transverse broadening as well as the longitudinal drag and longitudinal diffusion have been studied on an equal footing. We have categorically focused our study on "semihard" quarks where the mass and momentum scale as $M, p \sim \sqrt{\lambda} Q$, as these are the quarks for which mass modifications are most prominent. We have used power counting arguments loosely based on soft collinear effective theory (SCET) at various stages to isolate the leading contributions. It was shown in our earlier studies that both longitudinal and transverse momentum transfers have a comparable effect on the off-shellness of the heavy quark [37]. This earlier work implied that longitudinal transfers not only lead to the drag and diffusion, similar to light flavors, but will also noticeably affect the radiative energy loss and left strong indications that, for heavy quarks, the drag-induced radiation may be as significant as transverse momentum diffusion ($\hat{q}$) induced radiation.

In this paper we have explicitly demonstrated that the gluon bremsstrahlung spectrum from a semihard heavy quark is indeed strongly modified by drag-induced radiation. We have shown that due to the presence of the "−" light-cone momentum exchange from the medium (k^-), in our calculations, the

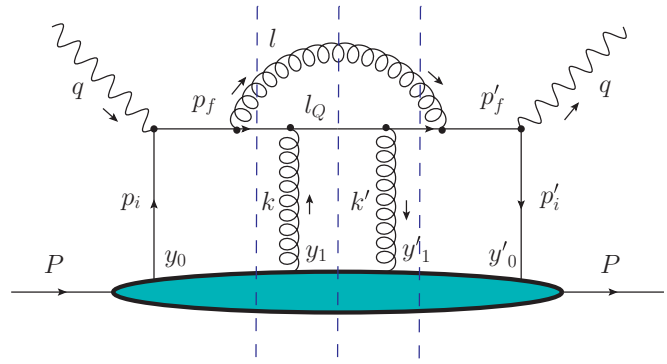

FIG. 3. Central, left and right cuts for $\mathcal{C}_{11}$.

definition of all the transport coefficients for heavy quark is different from that for light quark. Thus transport coefficients may indeed depend on properties of the probe, i.e., on mass or on the $l_\perp^2$. Whether this is phenomenologically significant cannot be ascertained at this point, and is left for a future investigation. This explicit dependence on the "−" light-cone momentum was absent in the limit of $k^- \to 0$, assumed in several prior calculations.

Analysis of the implications of the present study on the phenomenology of HIC is under way. In this work we have shown that the gluon bremsstrahlung spectrum of heavy quarks (unlike light quarks) is parametrically sensitive to $\hat{e}$, which quantifies the amount of drag the moving quark experiences. This result can be used to estimate the value of this subleading nonperturbative jet transport parameter ($\hat{e}$) from heavy flavor data of HIC experiments. These extra additive contributions may lead to an eventual solution of the heavy-quark puzzle. We leave these for a future effort.

ACKNOWLEDGMENTS

The authors would like to thank G.-Y. Qin for many helpful discussions. This work was supported in part by the National Science Foundation under Grant No. PHY-1207918. This work is also supported in part by the Director, Office of Energy Research, Office of High Energy and Nuclear Physics, Division of Nuclear Physics, of the U.S. Department of Energy, through the JET topical collaboration and also under Grant No. DE-SC0013460.

APPENDIX

There are three different cuts (central, left, and right) in Fig. 3 and their contributions are

$$\mathcal{C}_{11}^{c,l,r} = \frac{\alpha_s^2}{N_c}[C_F]\int dl_\perp^2 \left(\frac{1+(1-y)^2}{y}\right)\frac{[l_\perp^2+\kappa y^4 M^2]}{(l_\perp^2+y^2M^2)^2}\bar{I}_{11}^{c,l,r}, \tag{A1}$$

$$\bar{I}_{11}^{c} = \exp\left[i\left(x_B + x_L + \frac{x_M}{1-y}\right)P^+(y_0'^- - y_0^-)\right]\exp\left[i\left(\zeta x_D + (\zeta-1)\frac{x_M}{1-y} - \zeta\frac{\eta y^2}{1-y}x_L\right)P^+(y_1'^- - y_1^-)\right]\theta(y_0^- - y_1^-)$$
$$\times\theta(y_0'^- - y_1'^-)\left\{1 - \exp\left[-i\left(x_L + \frac{y}{1-y}x_M\right)P^+(y_1^- - y_0^-)\right]\right\}\left\{1 - \exp\left[i\left(x_L + \frac{y}{1-y}x_M\right)P^+(y_1'^- - y_0'^-)\right]\right\}, \tag{A2}$$

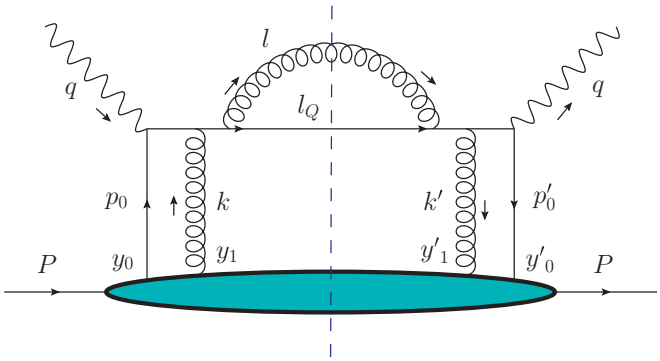

FIG. 4. Single possible central cut for $\mathcal{C}_{22}$.

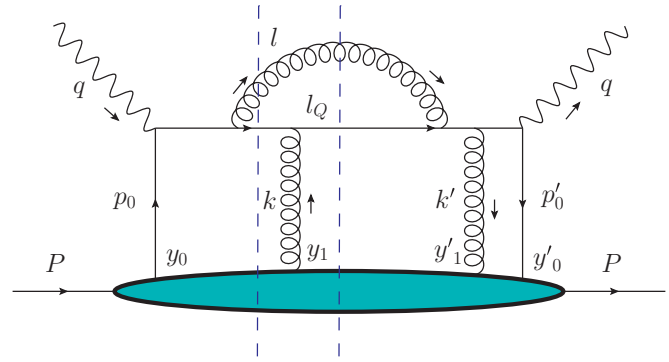

FIG. 5. Central and left cuts for $\mathcal{C}_{12}$.

$$\bar{I}^{l}_{11} = \exp\left[i\left(x_B + x_L + \frac{x_M}{1-y}\right)P^+(y_0'^- - y_0^-)\right]\exp\left[i\left(\zeta x_D + (\zeta-1)\frac{x_M}{1-y} - \zeta\frac{\eta y^2}{1-y}x_L\right)P^+(y_1'^- - y_1^-)\right]$$
$$\times\theta(y_1'^- - y_1^-)\theta(y_0'^- - y_1'^-)(-1)\left\{1 - \exp\left[i\left(x_L + \frac{y}{1-y}x_M\right)P^+(y_1'^- - y_0'^-)\right]\right\}, \tag{A3}$$

$$\bar{I}^{r}_{11} = \exp\left[i\left(x_B + x_L + \frac{x_M}{1-y}\right)P^+(y_0'^- - y_0^-)\right]\exp\left[i\left(\zeta x_D + (\zeta-1)\frac{x_M}{1-y} - \zeta\frac{\eta y^2}{1-y}x_L\right)P^+(y_1'^- - y_1^-)\right]\theta(y_0^- - y_1^-)$$
$$\times\theta(y_1^- - y_1'^-)\left\{1 - \exp\left[-i\left(x_L + \frac{y}{1-y}x_M\right)P^+(y_1^- - y_0^-)\right]\right\}(-1). \tag{A4}$$

In Fig. 4 there is only a central cut with the contribution

$$\mathcal{C}^{c}_{22} = \frac{\alpha_s^2}{N_c}[C_F]\int dl_\perp^2\left(\frac{1+\eta y + (1-y+\eta y)^2}{y}\right)\frac{[[(1+\eta y)l_\perp - yk_\perp]^2 + \kappa y^4M^2]}{[(l_\perp - yk_\perp)^2 + y^2M^2 + 2y\eta(l_\perp^2 - l_\perp k_\perp) + y^2\eta^2 l_\perp^2]^2}\bar{I}^{c,l,r}_{22}, \tag{A5}$$

$$\bar{I}^{c}_{22} = \exp\left[i\left(x_B + x_L + \frac{x_M}{1-y}\right)P^+(y_0'^- - y_0^-)\right]\exp\left[i\left(\zeta x_D + (\zeta-1)\frac{x_M}{1-y} - \zeta\frac{\eta y^2}{1-y}x_L\right)P^+(y_1'^- - y_1^-)\right]\theta(y_0^- - y_1^-)$$
$$\times\theta(y_0'^- - y_1'^-)\left\{-\exp\left[-i\left(x_L + \frac{y}{1-y}x_M\right)P^+(y_1^- - y_0^-)\right]\right\}\left\{-\exp\left[i\left(x_L + \frac{y}{1-y}x_M\right)P^+(y_1'^- - y_0'^-)\right]\right\}. \tag{A6}$$

In Fig. 5 there are two different cuts for induced gluon radiation, central and left:

$$\mathcal{C}^{c,l}_{12} = \frac{\alpha_s^2}{N_c}\left[-\left(C_F - \frac{C_A}{2}\right)\right]\int dl_\perp^2\left(\frac{1+(1-y)^2+\eta y(2-y)}{y}\right)$$
$$\times\frac{\{l_\perp[(1+\eta y)l_\perp - yk_\perp] + \kappa y^4M^2\}}{[l_\perp^2 + y^2M^2][(l_\perp - yk_\perp)^2 + y^2M^2 + 2y\eta(l_\perp^2 - l_\perp k_\perp) + y^2\eta^2 l_\perp^2]}\bar{I}^{c,l}_{12}, \tag{A7}$$

$$\bar{I}^{c}_{12} = \exp\left[i\left(x_B + x_L + \frac{x_M}{1-y}\right)P^+(y_0'^- - y_0^-)\right]\exp\left[i\left(\zeta x_D + (\zeta-1)\frac{x_M}{1-y} - \zeta\frac{\eta y^2}{1-y}x_L\right)P^+(y_1'^- - y_1^-)\right]\theta(y_0^- - y_1^-)$$
$$\times\theta(y_0'^- - y_1'^-)\left\{1 - \exp\left[-i\left(x_L + \frac{y}{1-y}x_M\right)P^+(y_1^- - y_0^-)\right]\right\}\left\{-\exp\left[i\left(x_L + \frac{y}{1-y}x_M\right)P^+(y_1'^- - y_0'^-)\right]\right\}, \tag{A8}$$

$$\bar{I}^{l}_{12} = \exp\left[i\left(x_B + x_L + \frac{x_M}{1-y}\right)P^+(y_0'^- - y_0^-)\right]\exp\left[i\left(\zeta x_D + (\zeta-1)\frac{x_M}{1-y} - \zeta\frac{\eta y^2}{1-y}x_L\right)P^+(y_1'^- - y_1^-)\right]$$
$$\times\theta(y_1'^- - y_1^-)\theta(y_0'^- - y_1'^-)\left\{\exp\left[i\left(x_L + \frac{y}{1-y}x_M\right)P^+(y_1^- - y_0'^-) + i(x_K - x_D)P^+(y_1'^- - y_1^-)\right]\right.$$
$$\left. - \exp\left[i\left(x_L + \frac{y}{1-y}x_M\right)P^+(y_1'^- - y_0'^-)\right]\right\}. \tag{A9}$$

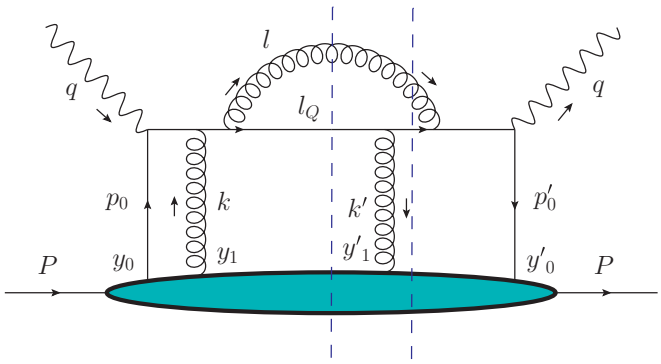

FIG. 6. Central and right cuts for $\mathcal{C}_{21}$.

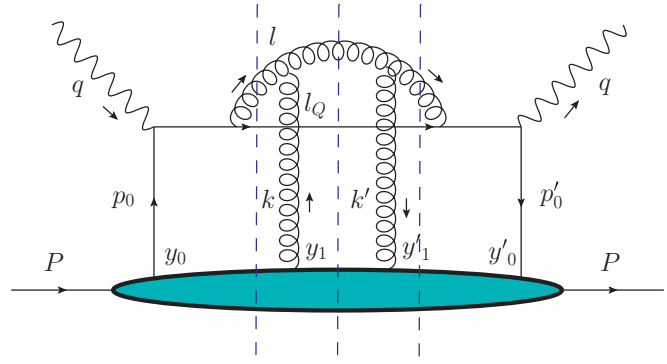

FIG. 7. Central, left and right cuts for $\mathcal{C}_{33}$.

In Fig. 6 there are two different cuts for induced gluon radition, central and right:

$$\mathcal{C}_{21}^{c,r} = \frac{\alpha_s^2}{N_c}\left[-\left(C_F - \frac{C_A}{2}\right)\right]\int dl_\perp^2\left(\frac{1+(1-y)^2+\eta y(2-y)}{y}\right)$$
$$\times\frac{\{[(1+\eta y)l_\perp - yk_\perp]l_\perp + \kappa y^4M^2\}}{[(l_\perp - yk_\perp)^2 + y^2M^2 + 2y\eta(l_\perp^2 - l_\perp k_\perp) + y^2\eta^2 l_\perp^2][l_\perp^2 + y^2M^2]}\bar{I}_{21}^{c,r},$$

$$\bar{I}_{21}^{c} = \exp\left[i\left(x_B + x_L + \frac{x_M}{1-y}\right)P^+(y_0'^- - y_0^-)\right]\exp\left[i\left(\zeta x_D + (\zeta-1)\frac{x_M}{1-y} - \zeta\frac{\eta y^2}{1-y}x_L\right)P^+(y_1'^- - y_1^-)\right]\theta(y_0^- - y_1^-)$$
$$\times\theta(y_0'^- - y_1'^-)\left\{-\exp\left[-i\left(x_L + \frac{y}{1-y}x_M\right)P^+(y_1^- - y_0^-)\right]\right\}\left\{1 - \exp\left[i\left(x_L + \frac{y}{1-y}x_M\right)P^+(y_1'^- - y_0'^-)\right]\right\}, \quad \text{(A10)}$$

$$\bar{I}_{21}^{r} = \exp\left[i\left(x_B + x_L + \frac{x_M}{1-y}\right)P^+(y_0'^- - y_0^-)\right]\exp\left[i\left(\zeta x_D + (\zeta-1)\frac{x_M}{1-y} - \zeta\frac{\eta y^2}{1-y}x_L\right)P^+(y_1'^- - y_1^-)\right]$$
$$\times\theta(y_1^- - y_1'^-)\theta(y_0^- - y_1^-)\left\{\exp\left[-i\left(x_L + \frac{y}{1-y}x_M\right)P^+(y_1'^- - y_0^-) - i(x_K - x_D)P^+(y_1^- - y_1'^-)\right]\right.$$
$$\left. - \exp\left[-i\left(x_L + \frac{y}{1-y}x_M\right)P^+(y_1^- - y_0^-)\right]\right\}. \quad \text{(A11)}$$

In Fig. 7 there are again all three possible cuts for induced gluon radition:

$$\mathcal{C}_{33}^{c} = \frac{\alpha_s^2}{N_c}[C_A]\int dl_\perp^2 P(y)\frac{[(l_\perp - k_\perp)^2 + \kappa y^4M^2]}{[(l_\perp - k_\perp)^2 + (1-\eta)^2y^2M^2]^2}\bar{I}_{33}^{c}$$

$$\bar{I}_{33}^{c} = \exp\left[i\left(x_B + x_L + \frac{x_M}{1-y}\right)P^+(y_0'^- - y_0^-)\right]\exp\left[i\left(\zeta x_D + (\zeta-1)\frac{x_M}{1-y} - \zeta\frac{\eta y^2}{1-y}x_L\right)P^+(y_1'^- - y_1^-)\right]\theta(y_0^- - y_1^-)$$
$$\times\theta(y_0'^- - y_1'^-)\left[\exp\left\{i\left(\frac{\zeta}{y(1-\eta)}x_D + \frac{\eta(1-y)}{(1-\eta)}x_L + (\zeta-1)\frac{x_M}{1-y} - \zeta\frac{\eta y^2}{1-y}x_L\right)P^+(y_1^- - y_0^-)\right\}\right.$$
$$\left. - \exp\left\{-i\left(x_L + \frac{y}{1-y}x_M\right)P^+(y_1^- - y_0^-)\right\}\right]\left[\exp\left\{-i\left(\frac{\zeta}{y(1-\eta)}x_D + \frac{\eta(1-y)}{(1-\eta)}x_L + (\zeta-1)\frac{x_M}{1-y} - \zeta\frac{\eta y^2}{1-y}x_L\right)\right.\right.$$
$$\left.\left.\times P^+(y_1'^- - y_0'^-)\right\} - \exp\left\{i\left(x_L + \frac{y}{1-y}x_M\right)P^+(y_1'^- - y_0'^-)\right\}\right],$$

$$\mathcal{C}_{33}^{l,r} = \frac{\alpha_s^2}{N_c}[C_A]\int dl_\perp^2 P(y)\frac{l_\perp^2 + \kappa y^4M^2}{[l_\perp^2 + y^2M^2]^2}\bar{I}_{33}^{l,r}, \quad \text{(A12)}$$

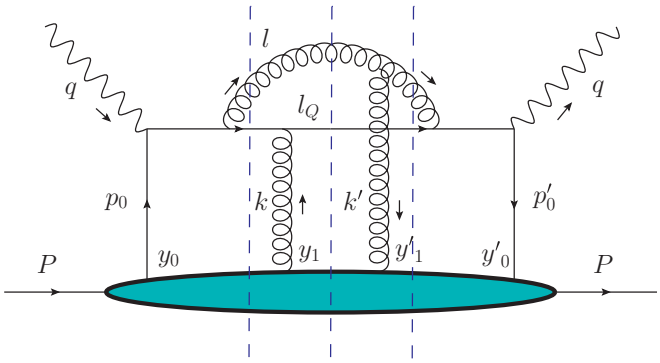

FIG. 8. Central, left and right cuts for $\mathcal{C}_{13}$.

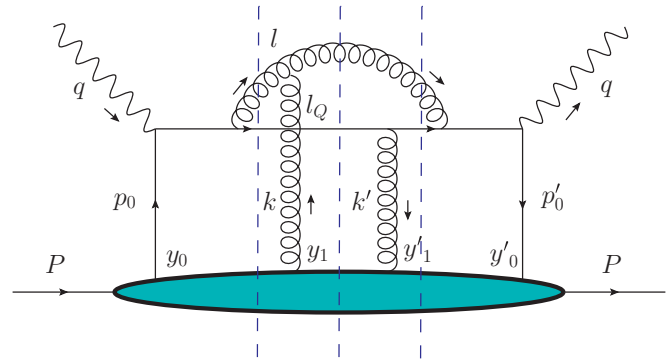

FIG. 9. Central, left and right cuts for $\mathcal{C}_{31}$.

$$\bar{I}^{l}_{33} = \exp\left[i\left(x_B + x_L + \frac{x_M}{1-y}\right)P^+(y_0'^- - y_0^-)\right]\exp\left[i\left(\zeta x_D + (\zeta-1)\frac{x_M}{1-y} - \zeta\frac{\eta y^2}{1-y}x_L\right)P^+(y_1'^- - y_1^-)\right]\theta(y_1'^- - y_1^-)$$
$$\times\theta(y_0'^- - y_1'^-)\left[-\exp\left\{i\left(\frac{-\zeta[1-2y(1-\eta)]}{y(1-\eta)}x_D - \frac{\eta(1-y)}{(1-\eta)}x_L + (\zeta-1)\frac{x_M}{1-y} - \zeta\frac{\eta y^2}{1-y}x_L\right)P^+(y_1^- - y_1'^-)\right\}\right]$$
$$\times\left\{1 - \exp\left[i\left(x_L + \frac{y}{1-y}x_M\right)P^+(y_1'^- - y_0'^-)\right]\right\}, \tag{A13}$$

$$\bar{I}^{r}_{33} = \exp\left[i\left(x_B + x_L + \frac{x_M}{1-y}\right)P^+(y_0'^- - y_0^-)\right]\exp\left[i\left(\zeta x_D + (\zeta-1)\frac{x_M}{1-y} - \zeta\frac{\eta y^2}{1-y}x_L\right)P^+(y_1'^- - y_1^-)\right]\theta(y_0^- - y_1^-)$$
$$\times\theta(y_1^- - y_1'^-)\left\{1 - \exp\left[-i\left(x_L + \frac{y}{1-y}x_M\right)P^+(y_1^- - y_0^-)\right]\right\}$$
$$\times\left[-\exp\left\{-i\left(\frac{-\zeta[1-2y(1-\eta)]}{y(1-\eta)}x_D - \frac{\eta(1-y)}{(1-\eta)}x_L + (\zeta-1)\frac{x_M}{1-y} - \zeta\frac{\eta y^2}{1-y}x_L\right)P^+(y_1'^- - y_1^-)\right\}\right]. \tag{A14}$$

There are also three cuts in Fig. 8, and the contributions are

$$\mathcal{C}^{c,l,r}_{13} = \frac{\alpha_s^2}{N_c}\left[-\frac{C_A}{2}\right]\int dl_\perp^2 P(y)\frac{[l_\perp(l_\perp - k_\perp) + \kappa y^4 M^2]}{[l_\perp^2 + y^2M^2][(l_\perp - k_\perp)^2 + y^2(1-\eta)^2M^2]}\bar{I}^{c,l,r}_{33}, \tag{A15}$$

$$\bar{I}^{c}_{13} = \exp\left[i\left(x_B + x_L + \frac{x_M}{1-y}\right)P^+(y_0'^- - y_0^-)\right]\exp\left[i\left(\zeta x_D + (\zeta-1)\frac{x_M}{1-y} - \zeta\frac{\eta y^2}{1-y}x_L\right)P^+(y_1'^- - y_1^-)\right]\theta(y_0^- - y_1^-)$$
$$\times\theta(y_0'^- - y_1'^-)\left\{1 - \exp\left[-i\left(x_L + \frac{y}{1-y}x_M\right)P^+(y_1^- - y_0^-)\right]\right\}\left[\exp\left\{-i\left(\frac{\zeta}{y(1-\eta)}x_D + \frac{\eta(1-y)}{(1-\eta)}x_L\right.\right.\right.$$
$$\left.\left.\left. + (\zeta-1)\frac{x_M}{1-y} - \zeta\frac{\eta y^2}{1-y}x_L\right)P^+(y_1'^- - y_0'^-)\right\} - \exp\left\{i\left(x_L + \frac{y}{1-y}x_M\right)P^+(y_1'^- - y_0'^-)\right\}\right], \tag{A16}$$

$$\bar{I}^{l}_{13} = \exp\left[i\left(x_B + x_L + \frac{x_M}{1-y}\right)P^+(y_0'^- - y_0^-)\right]\exp\left[i\left(\zeta x_D + (\zeta-1)\frac{x_M}{1-y} - \zeta\frac{\eta y^2}{1-y}x_L\right)P^+(y_1'^- - y_1^-)\right]\theta(y_1'^- - y_1^-)$$
$$\times\theta(y_0'^- - y_1'^-)(-1)\left[\exp\left\{-i\left(\frac{\zeta}{y(1-\eta)}x_D + \frac{\eta(1-y)}{(1-\eta)}x_L + (\zeta-1)\frac{x_M}{1-y} - \zeta\frac{\eta y^2}{1-y}x_L\right)P^+(y_1'^- - y_0'^-)\right\}\right.$$
$$\left. - \exp\left\{i\left(x_L + \frac{y}{1-y}x_M\right)P^+(y_1'^- - y_0'^-)\right\}\right], \tag{A17}$$

$$\bar{I}^{r}_{13} = \exp\left[i\left(x_B + x_L + \frac{x_M}{1-y}\right)P^+(y_0'^- - y_0^-)\right]\exp\left[i\left(\zeta x_D + (\zeta-1)\frac{x_M}{1-y} - \zeta\frac{\eta y^2}{1-y}x_L\right)P^+(y_1'^- - y_1^-)\right]\theta(y_0^- - y_1^-)$$
$$\times\theta(y_1'^- - y_1^-)\Bigg[\exp\left\{i\left(\frac{\zeta}{y(1-\eta)}x_D + \frac{\eta(1-y)}{(1-\eta)}x_L + (\zeta-1)\frac{x_M}{1-y} - \zeta\frac{\eta y^2}{1-y}x_L\right)P^+(y_1^- - y_0^-)\right\}$$
$$-\exp\left\{-i\left(x_L + \frac{y}{1-y}x_M\right)P^+(y_1^- - y_0^-)\right\}\Bigg]\Bigg[-\exp\left\{-i\left(\frac{-\zeta(1-2y(1-\eta))}{y(1-\eta)}x_D - \frac{\eta(1-y)}{(1-\eta)}x_L + (\zeta-1)\frac{x_M}{1-y}\right.\right.$$
$$\left.\left.-\zeta\frac{\eta y^2}{1-y}x_L\right)P^+(y_1'^- - y_1^-)\right\}\Bigg]. \tag{A18}$$

The contributions from the three cuts in Fig. 9 are

$$\mathcal{C}^{c,l,r}_{31} = \frac{\alpha_s^2}{N_c}\left[-\frac{C_A}{2}\right]\int dl_\perp^2 P(y)\frac{[(l_\perp - k_\perp)l_\perp + \kappa y^4 M^2]}{[(l_\perp - k_\perp)^2 + y^2(1-\eta)^2M^2][l_\perp^2 + y^2M^2]}\bar{I}^{c,l,r}_{31},$$

$$\bar{I}^{c}_{31} = \exp\left[i\left(x_B + x_L + \frac{x_M}{1-y}\right)P^+(y_0'^- - y_0^-)\right]\exp\left[i\left(\zeta x_D + (\zeta-1)\frac{x_M}{1-y} - \zeta\frac{\eta y^2}{1-y}x_L\right)P^+(y_1'^- - y_1^-)\right]\theta(y_0^- - y_1^-)$$
$$\times\theta(y_0'^- - y_1'^-)\Bigg[\exp\left\{i\left(\frac{\zeta}{y(1-\eta)}x_D + \frac{\eta(1-y)}{(1-\eta)}x_L + (\zeta-1)\frac{x_M}{1-y} - \zeta\frac{\eta y^2}{1-y}x_L\right)P^+(y_1^- - y_0^-)\right\}$$
$$-\exp\left\{-i\left(x_L + \frac{y}{1-y}x_M\right)P^+(y_1^- - y_0^-)\right\}\Bigg]\Bigg[1 - \exp\left\{i\left(x_L + \frac{y}{1-y}x_M\right)P^+(y_1'^- - y_0'^-)\right\}\Bigg], \tag{A19}$$

$$\bar{I}^{l}_{31} = \exp\left[i\left(x_B + x_L + \frac{x_M}{1-y}\right)P^+(y_0'^- - y_0^-)\right]\exp\left[i\left(\zeta x_D + (\zeta-1)\frac{x_M}{1-y} - \zeta\frac{\eta y^2}{1-y}x_L\right)P^+(y_1'^- - y_1^-)\right]\theta(y_0'^- - y_1'^-)$$
$$\times\theta(y_1'^- - y_1^-)\Bigg[-\exp\left\{-i\left(\frac{-\zeta[1-2y(1-\eta)]}{y(1-\eta)}x_D - \frac{\eta(1-y)}{(1-\eta)}x_L + (\zeta-1)\frac{x_M}{1-y} - \zeta\frac{\eta y^2}{1-y}x_L\right)P^+(y_1'^- - y_1^-)\right\}\Bigg]$$
$$\times\Bigg[\exp\left\{-i\left(\frac{\zeta}{y(1-\eta)}x_D + \frac{\eta(1-y)}{(1-\eta)}x_L + (\zeta-1)\frac{x_M}{1-y} - \zeta\frac{\eta y^2}{1-y}x_L\right)P^+(y_1'^- - y_0'^-)\right\}$$
$$-\exp\left\{i\left(x_L + \frac{y}{1-y}x_M\right)P^+(y_1'^- - y_0'^-)\right\}\Bigg], \tag{A20}$$

$$\bar{I}^{r}_{31} = \exp\left[i\left(x_B + x_L + \frac{x_M}{1-y}\right)P^+(y_0'^- - y_0^-)\right]\exp\left[i\left(\zeta x_D + (\zeta-1)\frac{x_M}{1-y} - \zeta\frac{\eta y^2}{1-y}x_L\right)P^+(y_1'^- - y_1^-)\right]\theta(y_1^- - y_1'^-)$$
$$\times\theta(y_0^- - y_1^-)(-1)\Bigg[\exp\left\{i\left(\frac{\zeta}{y(1-\eta)}x_D + \frac{\eta(1-y)}{(1-\eta)}x_L + (\zeta-1)\frac{x_M}{1-y} - \zeta\frac{\eta y^2}{1-y}x_L\right)P^+(y_1^- - y_0^-)\right\}$$
$$-\exp\left\{-i\left(x_L + \frac{y}{1-y}x_M\right)P^+(y_1^- - y_0^-)\right\}\Bigg]. \tag{A21}$$

Contributions from two cuts from Fig. 10 are as follows:

$$\mathcal{C}^{c}_{23} = \frac{\alpha_s^2}{N_c}\left[-\frac{C_A}{2}\right]\int dl_\perp^2\left(\frac{1+(1-y)^2}{y}\right)\frac{[(l_\perp - yk_\perp)(l_\perp - k_\perp) + \kappa y^4M^2]}{\left[(l_\perp - yk_\perp)^2 + y^2M^2 + 2y\left(\frac{k^-}{l^-}\right)l_\perp^2\right][(l_\perp - k_\perp)^2 + y^2(1-\eta)^2M^2]}\bar{I}^{c}_{23},$$

$$\bar{I}^{c}_{23} = \exp\left[i\left(x_B + x_L + \frac{x_M}{1-y}\right)P^+(y_0'^- - y_0^-)\right]\exp\left[i\left(\zeta x_D + (\zeta-1)\frac{x_M}{1-y} - \zeta\frac{\eta y^2}{1-y}x_L\right)P^+(y_1'^- - y_1^-)\right]$$
$$\times\,\theta(y_0^- - y_1^-)\theta(y_0'^- - y_1'^-)\Bigg\{-\exp\left[-i\left(x_L + \frac{y}{1-y}x_M\right)P^+(y_1^- - y_0^-)\right]\Bigg\}$$
$$\times\Bigg[\exp\left\{-i\left(\frac{\zeta}{y(1-\eta)}x_D + \frac{\eta(1-y)}{(1-\eta)}x_L + (\zeta-1)\frac{x_M}{1-y} - \zeta\frac{\eta y^2}{1-y}x_L\right)P^+(y_1'^- - y_0'^-)\right\}$$
$$-\exp\left\{i\left(x_L + \frac{y}{1-y}x_M\right)P^+(y_1'^- - y_0'^-)\right\}\Bigg], \tag{A22}$$

$$\mathcal{C}^{r}_{23} = \frac{\alpha_s^2}{N_c}\left[-\frac{C_A}{2}\right]\int dl_\perp^2\left(\frac{1+(1-y)^2}{y}\right)\frac{[l_\perp\{l_\perp - (1-y)k_\perp\} + \kappa y^4M^2]}{[l_\perp^2 + y^2M^2][\{l_\perp - (1-y)k_\perp\}^2 + y^2(1-\eta)^2M^2]}\bar{I}^{r}_{23}, \tag{A23}$$

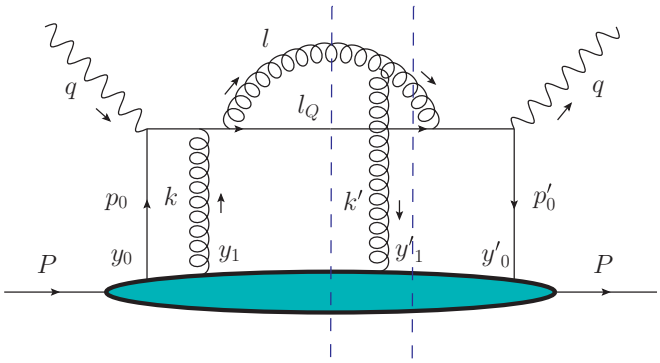

FIG. 10. Central and right cuts for $\mathcal{C}_{23}$.

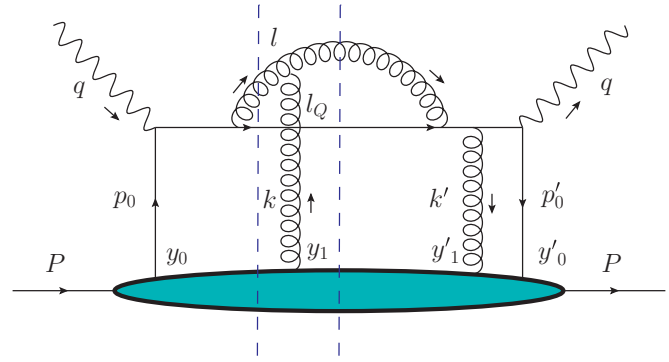

FIG. 11. Central and left cuts for $\mathcal{C}_{32}$.

$$\bar{I}^r_{23} = \exp\left[i\left(x_B + x_L + \frac{x_M}{1-y}\right)P^+(y_0'^- - y_0^-)\right]\exp\left[i\left(\zeta x_D + (\zeta-1)\frac{x_M}{1-y} - \zeta\frac{\eta y^2}{1-y}x_L\right)P^+(y_1'^- - y_1^-)\right]$$
$$\times\theta(y_1^- - y_1'^-)\theta(y_0^- - y_1^-)\left\{\exp\left[-i\left(x_L + \frac{y}{1-y}x_M\right)P^+(y_1'^- - y_0^-) - i(x_K - x_D)P^+(y_1^- - y_1'^-)\right]\right.$$
$$\left. - \exp\left[-i\left(\frac{-\zeta[1-2y(1-\eta)]}{y(1-\eta)}x_D - \frac{\eta(1-y)}{(1-\eta)}x_L\right)P^+(y_1'^- - y_1^-) - i\left(x_L + \frac{y}{1-y}x_M\right)P^+(y_1^- - y_0^-)\right]\right\}. \quad \text{(A24)}$$

Contributions of Fig. 11 are

$$\mathcal{C}^c_{32} = \frac{\alpha_s^2}{N_c}\left[\frac{C_A}{2}\right]\int dl_\perp^2\left(\frac{1+(1-y)^2}{y}\right)\frac{[(l_\perp - k_\perp)(l_\perp - yk_\perp) + \kappa y^4M^2]}{[(l_\perp - k_\perp)^2 + y^2(1-k^-/l^-)^2M^2]\left[(l_\perp - yk_\perp)^2 + y^2M^2 + 2y\left(\frac{k^-}{l^-}\right)l_\perp^2\right]}\bar{I}^c_{32}, \quad \text{(A25)}$$

$$\bar{I}^c_{32} = \exp\left[i\left(x_B + x_L + \frac{x_M}{1-y}\right)P^+(y_0'^- - y_0^-)\right]\exp\left[i\left(\zeta x_D + (\zeta-1)\frac{x_M}{1-y} - \zeta\frac{\eta y^2}{1-y}x_L\right)P^+(y_1'^- - y_1^-)\right]\theta(y_0^- - y_1^-)$$
$$\times\theta(y_0'^- - y_1'^-)\left[\exp\left\{i\left(\frac{\zeta}{y(1-\eta)}x_D + \frac{\eta(1-y)}{(1-\eta)}x_L + (\zeta-1)\frac{x_M}{1-y} - \zeta\frac{\eta y^2}{1-y}x_L\right)P^+(y_1^- - y_0^-)\right\}\right.$$
$$\left. - \exp\left\{-i\left(x_L + \frac{y}{1-y}x_M\right)P^+(y_1^- - y_0^-)\right\}\right]\left[-\exp\left\{i\left(x_L + \frac{y}{1-y}x_M\right)P^+(y_1'^- - y_0'^-)\right\}\right], \quad \text{(A26)}$$

$$\mathcal{C}^l_{32} = \frac{\alpha_s^2}{N_c}\left[\frac{C_A}{2}\right]\int dl_\perp^2\left(\frac{1+(1-y)^2}{y}\right)\frac{[\{l_\perp - (1-y)k_\perp\}l_\perp + \kappa y^4M^2]}{[(l_\perp - k_\perp)^2 + y^2(1-\eta)^2M^2][(l_\perp - yk_\perp)^2 + y^2M^2 + 2y\eta l_\perp^2]}\bar{I}^l_{32}, \quad \text{(A27)}$$

$$\bar{I}^l_{32} = \exp\left[i\left(x_B + x_L + \frac{x_M}{1-y}\right)P^+(y_0'^- - y_0^-)\right]\exp\left[i\left(\zeta x_D + (\zeta-1)\frac{x_M}{1-y} - \zeta\frac{\eta y^2}{1-y}x_L\right)P^+(y_1'^- - y_1^-)\right]$$
$$\times\theta(y_1'^- - y_1^-)\theta(y_0'^- - y_1'^-)(-1)\left[\exp\left\{i\left(x_L + \frac{y}{1-y}x_M\right)P^+(y_1^- - y_0'^-) + i(x_K - x_D)P^+(y_1'^- - y_1^-)\right\}\right.$$
$$\left. - \exp\left\{i\left(\frac{-\zeta(1-2y(1-\eta))}{y(1-\eta)}x_D - \frac{\eta(1-y)}{(1-\eta)}x_L\right)P^+(y_1^- - y_1'^-) + i\left(x_L + \frac{y}{1-y}x_M\right)P^+(y_1'^- - y_0'^-)\right\}\right]. \quad \text{(A28)}$$

Figure 12 has one possible cut,

$$\mathcal{C}^l_{10} = \frac{\alpha_s^2}{N_c}[C_F]\int dl_\perp^2 P(y)\frac{[l_\perp^2 + \kappa y^4M^2]}{(l_\perp^2 + y^2M^2)^2}\bar{I}^l_{10}, \quad \text{(A29)}$$

$$\bar{I}^l_{10} = \exp\left[i\left(x_B + x_L + \frac{x_M}{1-y}\right)P^+(y_0'^- - y_0^-)\right]\exp\left[i\left(\zeta x_D + (\zeta-1)\frac{x_M}{1-y} - \zeta\frac{\eta y^2}{1-y}x_L\right)P^+(y_1'^- - y_1^-)\right]\theta(y_1'^- - y_1^-)$$
$$\times\theta(y_0'^- - y_1'^-)\left\{-\exp[-i(x_K - x_D)P^+(y_1'^- - y_1^-)]\exp\left[i\left(x_L + \frac{y}{1-y}x_M\right)P^+(y_1^- - y_0'^-)\right]\right\}. \quad \text{(A30)}$$

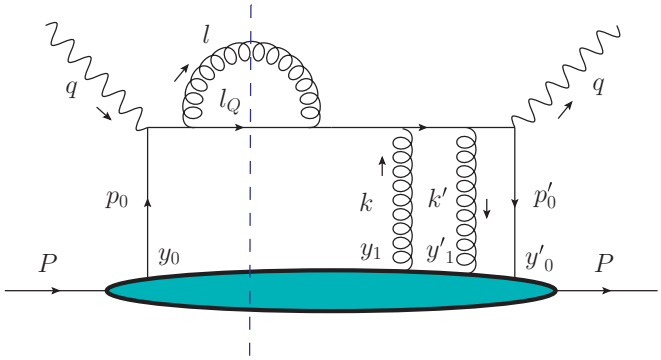

FIG. 12. Single possible right cut for $\mathcal{C}_{01}$.

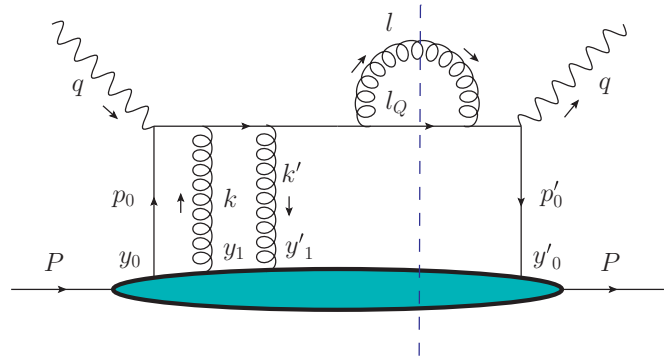

FIG. 13. Single possible left cut for $\mathcal{C}_{10}$.

Figure 13 also has single possible cut,

$$\mathcal{C}^r_{01} = \frac{\alpha_s^2}{N_c}[C_F]\int dl_\perp^2 P(y)\frac{[l_\perp^2+\kappa y^4 M^2]}{(l_\perp^2+y^2M^2)^2}\bar{I}^r_{10}, \tag{A31}$$

$$\bar{I}^r_{01} = \exp\left[i\left(x_B+x_L+\frac{x_M}{1-y}\right)P^+(y_0'^- - y_0^-)\right]\exp\left[i\left(\zeta x_D+(\zeta-1)\frac{x_M}{1-y}-\zeta\frac{\eta y^2}{1-y}x_L\right)P^+(y_1'^- - y_1^-)\right]$$
$$\times\theta(y_1'^- - y_1^-)\theta(y_0'^- - y_1'^-)\left\{-\exp[i(x_K-x_D)P^+(y_1'^- - y_1^-)]\exp\left[-i\left(x_L+\frac{y}{1-y}x_M\right)P^+(y_1'^- - y_0^-)\right]\right\}. \tag{A32}$$

[1] X. N. Wang and M. Gyulassy, Phys. Rev. Lett. **68**, 1480 (1992).
[2] M. Gyulassy and X. N. Wang, Nucl. Phys. B **420**, 583 (1994).
[3] R. Baier, Y. L. Dokshitzer, A. H. Mueller, S. Peigne, and D. Schiff, Nucl. Phys. B **483**, 291 (1997).
[4] B. G. Zakharov, JETP Lett. **63**, 952 (1996).
[5] A. Majumder and M. Van Leeuwen, Prog. Part. Nucl. Phys. A **66**, 41 (2011).
[6] U. A. Wiedemann, in *Relativistic Heavy Ion Physics*, edited by R. Stock, Landolt-Börnstein, Numerical Data and Functional Relationships in Science and Technology, New Series, Vol. 23 (Springer, Berlin, 2010), p. 521.
[7] N. Armesto, B. Cole, C. Gale, W. A. Horowitz, P. Jacobs, S. Jeon, M. van Leeuwen, A. Majumder *et al.*, Phys. Rev. C **86**, 064904 (2012).
[8] G. Y. Qin and A. Majumder, Phys. Rev. Lett. **105**, 262301 (2010).
[9] M. Djordjevic, Phys. Rev. Lett. **112**, 042302 (2014).
[10] B. I. Abelev *et al.* (STAR Collaboration), Phys. Rev. Lett. **98**, 192301 (2007); **106**, 159902 (2011).
[11] A. Adare *et al.* (PHENIX Collaboration), Phys. Rev. Lett. **98**, 172301 (2007).
[12] M. Djordjevic and M. Gyulassy, Nucl. Phys. A **733**, 265 (2004).
[13] M. Djordjevic, M. Gyulassy, and S. Wicks, Phys. Rev. Lett. **94**, 112301 (2005).
[14] B. Abelev *et al.* (ALICE Collaboration), J. High Energy Phys. 09 (2012) 112.
[15] K. Aamodt *et al.* (ALICE Collaboration), Phys. Lett. B **696**, 30 (2011).
[16] M. Djordjevic and M. Djordjevic, Phys. Rev. C **90**, 034910 (2014).
[17] M. G. Mustafa, Phys. Rev. C **72**, 014905 (2005).
[18] S. Wicks, W. Horowitz, M. Djordjevic, and M. Gyulassy, Nucl. Phys. A **784**, 426 (2007).
[19] R. Abir, C. Greiner, M. Martinez, M. G. Mustafa, and J. Uphoff, Phys. Rev. D **85**, 054012 (2012).
[20] R. Abir, U. Jamil, M. G. Mustafa, and D. K. Srivastava, Phys. Lett. B **715**, 183 (2012).
[21] B. W. Zhang, E. K. Wang, and X. N. Wang, Nucl. Phys. A **757**, 493 (2005).
[22] M. He, R. J. Fries, and R. Rapp, Nucl. Phys. A **910–911**, 409 (2013).
[23] S. Cao and S. A. Bass, Phys. Rev. C **84**, 064902 (2011).
[24] G. D. Moore and D. Teaney, Phys. Rev. C **71**, 064904 (2005).
[25] R. Baier, Nucl. Phys. A **715**, 209c (2003).
[26] A. Majumder, Phys. Rev. C **87**, 034905 (2013).
[27] A. Majumder, Phys. Rev. C **80**, 031902 (2009).
[28] A. Majumder and B. Muller, Phys. Rev. C **77**, 054903 (2008).
[29] G. Y. Qin and A. Majumder, Phys. Rev. C **91**, 044906 (2015).
[30] P. B. Arnold, G. D. Moore, and L. G. Yaffe, J. High Energy Phys. 06 (2002) 030.
[31] S. Jeon and G. D. Moore, Phys. Rev. C **71**, 034901 (2005).
[32] N. Armesto, C. A. Salgado, and U. A. Wiedemann, Phys. Rev. D **69**, 114003 (2004).
[33] C. W. Bauer, S. Fleming, D. Pirjol, and I. W. Stewart, Phys. Rev. D **63**, 114020 (2001).
[34] C. W. Bauer and I. W. Stewart, Phys. Lett. B **516**, 134 (2001).
[35] C. W. Bauer, D. Pirjol, and I. W. Stewart, Phys. Rev. D **65**, 054022 (2002).
[36] C. W. Bauer, S. Fleming, D. Pirjol, I. Z. Rothstein, and I. W. Stewart, Phys. Rev. D **66**, 014017 (2002).
[37] R. Abir, G. D. Kaur, and A. Majumder, Phys. Rev. D **90**, 114026 (2014).

[38] A. Idilbi and A. Majumder, Phys. Rev. D **80**, 054022 (2009).
[39] F. D'Eramo, H. Liu, and K. Rajagopal, Phys. Rev. D **84**, 065015 (2011).
[40] G.-Y. Qin and A. Majumder, Phys. Rev. C **87**, 024909 (2013).
[41] Y. L. Dokshitzer and D. E. Kharzeev, Phys. Lett. B **519**, 199 (2001).
[42] X. N. Wang and X. F. Guo, Nucl. Phys. A **696**, 788 (2001).
[43] L. D. Landau and I. Pomeranchuk, Dokl. Akad. Nauk Ser. Fiz. **92**, 535 (1953).
[44] A. B. Migdal, Phys. Rev. **103**, 1811 (1956).
[45] A. Majumder, Phys. Rev. D **85**, 014023 (2012).